

Catalyzed growth of encapsulated carbyne

Umedjon Khalilov*, Charlotte Vets, Erik C. Neyts

PLASMANT Research Group, Department of Chemistry, University of Antwerp, Universiteitsplein 1, 2610, Antwerp, Belgium



ARTICLE INFO

Article history:

Received 19 April 2019

Received in revised form

28 June 2019

Accepted 30 June 2019

Available online 1 July 2019

ABSTRACT

Carbyne is a novel material of current interest in nanotechnology. As is typically the case for nano-materials, the growth process determines the resulting properties. While endohedral carbyne has been successfully synthesized, its catalyst and feedstock-dependent growth mechanism is still elusive. We here study the nucleation and growth mechanism of different carbon chains in a Ni-containing double walled carbon nanotube using classical molecular dynamics simulations and first-principles calculations. We find that the understanding the competitive role of the metal catalyst and the hydrocarbon is important to control the growth of 1-dimensional carbon chains, including Ni or H-terminated carbyne. Also, we find that the electronic property of the Ni-terminated carbyne can be tuned by steering the H concentration along the chain. These results suggest catalyst-containing carbon nanotubes as a possible synthesis route for carbyne formation.

© 2019 Elsevier Ltd. All rights reserved.

1. Introduction

Carbyne is a 1D carbon allotrope [1]; it is an infinitely long linear chain of *sp*-hybridized carbon atoms with extraordinary properties [2–4]. Specifically its mechanical properties such as the Young modulus (32.71 TPa), shear modulus (11.8 TPa), and specific stiffness (about 10^9 N m/kg) significantly outperform any other material including carbon nanotubes, graphene and diamond [5]. Also, its very high thermal conductivity (80 kW/m·K at room temperature) [6], structure-dependent electronic [7] and other properties are very attractive [8,9].

Carbyne is produced using various growth techniques including arc discharge [10–12], laser ablation [3,13], on-surface synthesis [14,15], electrochemical synthesis [16] and others [17,18]. However, the synthesis of long carbyne is extremely difficult due to its high chemical reactivity and instability [10,19]. Nevertheless, such long carbon chains have successfully been obtained to some extent [11,20,21]. Especially, the inner space of carbon nanotubes has been recognized as an ideal location for the carbyne chain [19,22] and thus the endohedral carbyne growth is actively being investigated. In particular, spontaneous formation of linear carbon chains with several tens of C atoms in double walled carbon nanotube (DWNT)

has been observed through insertion of precursor molecules, e.g., polyyne C_nH_2 molecules [20] and adamantane ($C_{10}H_{16}$) [21]. Also, Zhao and colleague reported long linear C chain more than 100 carbon atoms inside multi-walled carbon nanotube (MWNT) obtained by hydrogen arc discharge evaporation of carbon rods [12]. Recently, Shi et al. have experimentally grown record-long carbyne chain with 6000 C atoms inside a DWNT [22]. Several investigations indicate that the high-temperature treatment of MWNT, especially DWNT with suitable innermost diameter allows for the synthesis of long carbon chains [19,22,23].

In the formation of endohedral carbyne from hydrocarbon species, a metal catalyst can facilitate bond breaking and C–C bond formation after feedstock adsorption by decreasing the activation energy barriers of these reactions. In particular, transition metals are used as a catalyst in the steam methane reforming for producing syngas [24], in the Fischer-Tropsch reactions for producing hydrocarbons [25], in the synthesis of nanostructures using chemical vapor deposition technique [26], etc. However, the metal-catalyzed growth of the encapsulated carbyne is not reported yet. Consequently, the growth mechanism, and the role of the catalyst and the feedstock for the case of endohedral carbyne synthesis are still elusive. In order to elucidate these phenomena, we here study the Ni-catalyzed nucleation and growth of carbon chains in DWNT from carbon (C_2) and hydrocarbon (C_2H or C_2H_2) species, using both reactive Molecular Dynamics (MD) simulations and Density Functional Theory (DFT) calculations.

* Corresponding author.

E-mail address: umedjon.khalilov@uantwerpen.be (U. Khalilov).

2. Computational methodology

In the reactive MD simulations, we use the ReaxFF potential [27] with parameters developed by Zou et al. [28]. To grow the endohedral carbyne a (5,5)@(10,10) DWNT is chosen, as shown in Fig. 1. The inner (d_{in}) and outer (d_{out}) diameters of the DWNT are 0.70 nm and 1.39 nm, respectively. These values are in agreement with experimentally reported tube diameters, viz. $0.63 \text{ nm} < d_{in} < 0.79 \text{ nm}$ and $1.3 \text{ nm} < d_{out} < 1.6 \text{ nm}$ [29]. Also, the inner (5,5) nanotube with diameter of about 0.7 nm is optimal to stabilize a carbon chain, in very good agreement with experiments as well [19,20,22]. Periodicity is applied along the z-axis, mimicking an infinitely long DWNT. Subsequently, Ni atoms are inserted in the inner tube, mimicking the experimental embedded Ni nanoclusters in carbon nanotubes [30]. Due to weak Ni–C π bonds, endohedral Ni-atoms can easily move on the tube wall.

The simulated system is initially equilibrated at the desired temperature applying the Berendsen thermostat [31] in the NpT ensemble. Subsequently, the Bussi thermostat [32] is used to control the temperature in the canonical NVT simulations. During the simulations, the chosen growth species, i.e., C_2 , C_2H and C_2H_2 are inserted in the inner tubewith an interval of 25 ps and 250 ps at high (1700 K) and low (500 K) temperatures, respectively. In general, the tube diameters and growth temperatures are chosen according to theoretical suggestions and experimental findings [33].

All DFT calculations are carried out using the VASP software [34,35]. All optimizations are carried out at in the generalized gradient approximation (GGA), employing the revised Perdew-Burke-Ernzerhof (RPBE) functional [36]. All calculations employ the projector augmented wave method (PAW) [37,38], Gaussian smearing [39,40], and a Γ -centered ($1 \times 1 \times 1$) k-point mesh, with supercells of size ($20 \times 20 \times 20$) Å. We employ spin polarization and no symmetry constraints. The energy cutoff is set to 400 eV and the energy convergence is set to 1×10^{-4} eV. While the van der Waals corrections are not included in DFT calculations, test calculations including van der Waals interactions (using the Perdew-Burke-Ernzerhof (PBE) functional [41,42] and the Tkatchenko-Scheffler method [43]) indicate that the effect is negligible.

3. Results and discussion

The nucleation and growth steps of Ni-catalyzed endohedral

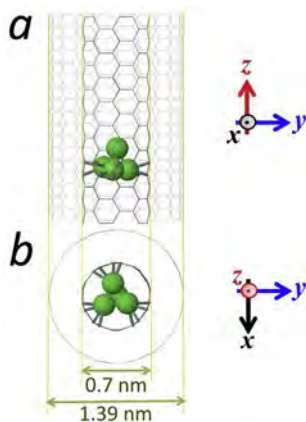


Fig. 1. Front (a) and top view (b) of Ni-containing (5,5)@(10,10) double-walled carbon nanotubes (DWNTs). In sake of clarity, carbon atoms in DWNT are not shown: light and dark grey wire frames are outer and inner walls of DWNT, respectively. Ni atoms are in green color. (A colour version of this figure can be viewed online.)

carbyne from carbon (C_x) and hydrocarbon (C_xH_y) species are depicted in Fig. 2. The simulations show that the sticking probability and the adsorption energies of new-inserted feedstock on the metal cluster inversely depend on the ratio of N_H/N_C . The adsorption energies are seen to decrease with increasing N_H/N_C ratio in the feedstock. While the absolute value of the adsorption energies in DFT and MD differ by a factor of almost 2 (-3.68 , -2.88 eV and -1.36 eV for C_2 , C_2H and C_2H_2 , respectively, in MD, vs. -6.43 eV, -5.14 eV and -1.91 eV for DFT), the trend is maintained.

When the inserted molecule impinges on the metal nanocluster either (1) it connects to another adsorbed molecule or (2) it gradually loses its H atoms at the high or low feedstock pressure (flux) conditions, respectively. In the first case (dimerization), the adsorbed feedstocks molecules directly associate on the nanocluster, prior to breaking their C–H bonds, as is demonstrated in Fig. 3. MD-NEB calculations [44] show that the formation of initial carbon chains from the feedstock dimerization requires association activation barriers of about 0.1 eV, 0.26 eV and 0.3 eV for C_2 , C_2H and C_2H_2 , respectively.

In the second case (dehydrogenation), C–H bonds of the adsorbed molecule are gradually broken. In particular, in the case of acetylene (C_2H_2), its two C–C π bonds can each be broken to form Ni–C σ bonds as it chemisorbs (without fragmenting) to the nickel cluster. In the case that the molecule connects to a single Ni atom, however, one π bond remains such that a double C–C bond is retained (e.g., see Fig. 2c, frame 2). The adsorbed molecule begins dehydrogenating to form ethynyl radical (C_2H) and it subsequently decomposes to a C_2 dimer and a H atom. While the C–C bonds break before C–H bonds on a flat Ni(111) surface, the presence of steps on the surface lowers the activation barrier for C–H bond cleavage [45]. Our Ni nanoparticle behaves like the stepped surface rather than the flat surface and it thus preferably breaks C–H bond instead of the C–C bond. It indicates that the dissociation of the adsorbed feedstock occurs through step-wise dehydrogenation [24], i.e., $C_2H_2 \Rightarrow C_2H \Rightarrow C_2$. In moderate pressure cases, dehydrogenation and dimerization can simultaneously occur. In all cases, consecutive carbon (with or without hydrogen) connections eventually initiate the formation of the incipient carbon chain (Fig. 2, second and third columns). The total energy of the carbon chain gradually decreases when the carbon concentration increases in the carbon chain. In particular, the change in the system energy per C addition is -6.42 eV, which is very close to the DFT values ranging between -5.77 eV and -7.67 eV for finite carbyne [3,5,46].

In the C_x case, the continuous extension of the chain length induces the nanocluster to split into two smaller fragments, which bind respectively at both ends of the carbon chain (see Fig. 2a, frame 3). The termination by Ni atoms as well as van der Waals interaction with the inner tube facilitates the carbyne growth. While such end-terminations preferable occur, we do not find the carbon chain is embedded into the cluster during the simulations [47]. Due to the Ni-termination of both ends, the undesired connection of the carbyne with the tube wall does not occur. When a single Ni atom is used as a catalyst, however, the interaction probability of the catalyst-free end of the carbyne with the tube wall significantly increases. Similar experimental observations were reported by Kano et al., i.e., when one Pt atom connects to one end of the obtained carbon chain on a graphene flake, its Pt-free end becomes very unstable [14]. Consequently, chain-tube connections may result in a considerable reduction of the carbyne growth and defect creation in the host tube [11]. While the termination of both ends of the carbyne chain is required in the growth from C_x growth species, the carbyne ends are devoid of such chain-tube influence during the growth from hydrocarbon (C_xH_y)

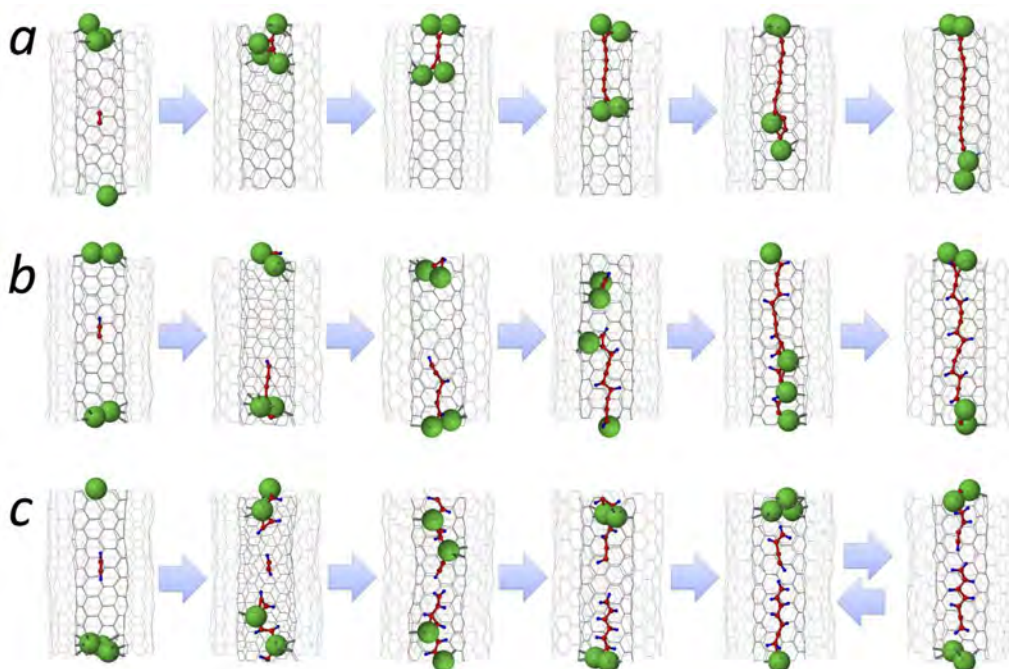


Fig. 2. Ni-assisted carbyne nucleation and growth in a (5,5)@(10,10) tube from C_2 (a), C_2H (b) and C_2H_2 (c) precursors. Inserted C and H atoms are highlighted in red and blue colors, respectively. (A colour version of this figure can be viewed online.)

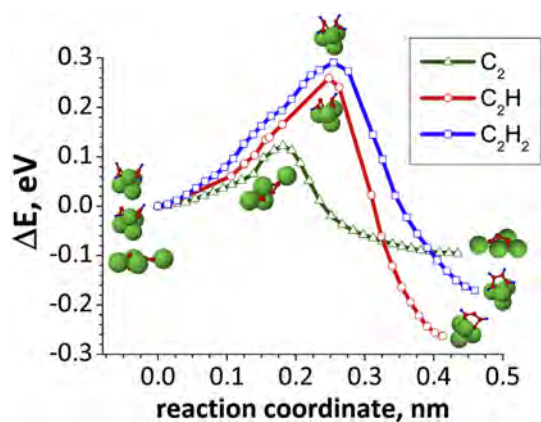


Fig. 3. Association/dissociation steps and activation barriers in the onset of Ni-assisted nucleation of carbon chain from C_2 (green line with open triangles), C_2H (red line with open circles) and C_2H_2 (blue line with open squares) feedstocks. (A colour version of this figure can be viewed online.)

feedstocks. Namely, the catalyst-free carbyne tail is quickly terminated by a H atom and undesirable reactions are thus prevented (Fig. 2b and c, second and third columns), indicating that in this case the single Ni atom could also be applied as a catalyst in the growth process.

The overall results indicate that catalyst and hydrogen have opposite effects during the chain nucleation and growth. Namely, the catalyst facilitates the formation of C–C connections and thus enhances the chain elongation. In contrast, hydrogen quickly blocks the chain tail and thus delays or prevents continued chain growth. In the Ni_n cluster case, both catalyst and hydrogen atoms can move along the growing chain as well. Due to this phenomenon, the catalyst atom is seen to bind to the tail of the chain terminated by H

and stimulates the chain to grow again (Fig. 2b, third, fourth and fifth columns). Consequently, the obtained carbon chains can be partially or fully hydrogenated and terminated by nickel and/or hydrogen atoms.

In the growth processes, we find several types of carbon chains, viz., polyyne, cumulene and polyene chains [48] with complete or

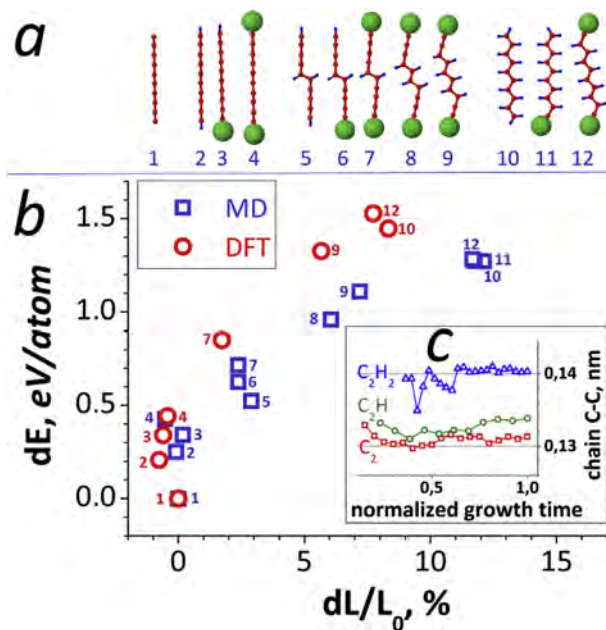


Fig. 4. (a) Possible chain structures in the catalyzed growth; (b) Dependence of the energy change on the relative extension of chain length; (c) Average C–C bond length during the growth from C_2 , C_2H and C_2H_2 feedstocks.

partial termination by metal or hydrogen atom(s), as demonstrated in Fig. 4a.

Every model structure contains 10 C atoms. The aforementioned simulation results indicate in the case of C_2 feedstock that the obtained metal-terminated chain is cumulene-like ($\dots =C=C=C=$) (see structure 4 in Fig. 4a) with a bond distance (r) of about 0.13 nm (see C_2 in Fig. 4c), which is very close to the experimental value (0.131 nm) for the C–C bond length in a metalated carbyne [15]. Normally, carbyne favours a polyene structure ($\dots -C\equiv C-C\equiv C- \dots$) with C–C bond length alternation (BLA = $|r_1-r_2|$) due to the Peierls instability. However, zero-point atomic vibrations eliminate such bond alternation making the cumulene C_n chain a stable carbyne structure as well [49]. According to DFT calculations, the energy difference between polyene and cumulene structures is 2 meV per carbon [5]. At absolute zero, therefore, the carbyne chain is polyene-like, e.g., in our MD calculations the BLA is 14 pm ($r_1/r_2 = 0.12/0.134$). While this value is higher than our DFT value of 3 pm ($r_1/r_2 = 0.128/0.131$), it is in close agreement with the experimental value, i.e., BLA = 10 pm ($r_1/r_2 = 0.123/0.133$). At non-zero temperature, the BLA tends to zero due to the temperature-dependent chain fluctuations. In addition, such polyene-cumulene transitions occur due to changing H-termination to H_2 -termination [48] or due to the elongation of the chain length [49]. The length of the carbon chain relatively extends depending on the degree of hydrogenation of the chain, i.e., the average C–C bond in the chains for the C_2 , C_2H and C_2H_2 cases are 0.13 nm, 0.134 nm and 0.14 nm, respectively (Fig. 4c). Also, the connection of the catalyst atom(s) or/and H atom(s) to the carbon chain can affect both its length and stability. While the length of Ni or H-terminated carbyne structures does not alter significantly, their relative potential energy decreases somewhat (see 1–4 in Fig. 4b). Note that Ni atoms have the positive partial charges (oxidation state of Ni is maximum +2) and consequently the neighboring C atoms have negative partial charges due to partially ionic character of the Ni–C bond. The total charge of the structures is zero in both MD and DFT calculations. On the other hand, both length and stability of hydrogenated carbon chains terminated by either Ni/Ni (structures 4, 7–9, 12 in Fig. 4a) or Ni/H (structures 3, 6, 11 in Fig. 4a) or H/H (structures 2, 5, 10 in Fig. 4a) increase by increasing the H concentration in the chain (see 5–12 in Fig. 4b). Also, consecutive H addition leads the transformation of the chain structure from a “linear” cumulene/polyene allotrope to a “zigzag” polyene structure [48]. Such additions do not only alter the morphology of the structures, they can change the electronic property of the obtained

carbon chains as well.

Fig. 5 a shows the calculated density of states (DOS) from -5.0 eV to 5.0 eV, for four carbon chains, i.e., structures 1, 4, 7 and 12 from Fig. 4a. The figure shows that different structures have different gap. As our carbyne structure is calculated as a non-periodic structure, the DOS looks different from other works [49,50], where only one (large) band gap (around 2.20 eV) can be observed for those periodic carbyne structures. However, our gap values are close to ab-initio calculation results for confined carbon chains [17,51]. The gap widths for each structure are shown separately in Fig. 5b. The figures indicate that the most prominent gap (1.25 eV) appears in case of a finite carbyne (structure 1). When the ends of the carbyne chain are terminated by Ni atoms (structure 4), this prominent gap considerably decreases to 0.69 eV (–45%). Subsequently, this gap decreases further when H atoms are added along the carbyne chain. In particular, maximum gap widths for Ni-terminated carbyne with 2 H atoms (structure 7) and Ni-terminated carbyne with 8 H atoms (structure 12) are 0.62 eV (–50%) and 0.16 eV (–88%), respectively. Indeed, Fig. 5 demonstrates that the overall gap widths significantly decrease when H atoms are added along the Ni-terminated carbyne chain, as the dispersion moves towards smaller values.

4. Conclusion

We study the Ni-catalyzed growth of carbyne inside a double-walled carbon nanotube from carbon and hydrocarbon feedstocks using MD simulations and DFT calculations. We find that a confined long carbyne can be grown from carbon species assisted by Ni as a catalyst. However, in the case of growth from hydrocarbon species, the carbyne chain growth can be hindered by the H addition. Competition between the metal and hydrogen results in various Ni or H-terminated carbon chains with varying degrees of hydrogenation in the tube. The length and stability of the grown chains are also dependent on the type of chain termination and the degree of hydrogenation. We also find that the band gap in metal-terminated carbyne is significantly decreased when H atoms adsorbed along the chain. The overall simulation/calculation results are in agreement with available experimental and theoretical evidences and strongly indicate that the formation of finite carbyne structure with controllable electronic properties is possible.

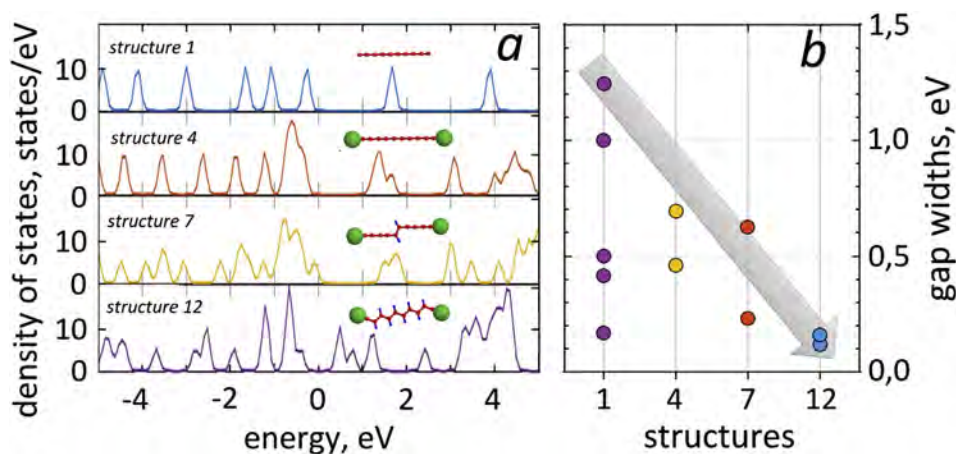


Fig. 5. (a) Density of states (DOS) and (b) gap dispersion in DOS for various carbon chains.

Acknowledgements

The authors gratefully acknowledge the financial support from the Fund of Scientific Research Flanders (FWO), Belgium, Grant numbers 12M1318N and 1S22516N. The work was carried out in part using the Turing HPC infrastructure of the CalcUA core facility of the Universiteit Antwerpen, a division of the Flemish Super-computer Centre VSC, funded by the Hercules Foundation, the Flemish Government (department EWI) and the University of Antwerp.

Appendix A. Supplementary data

Supplementary data to this article can be found online at <https://doi.org/10.1016/j.carbon.2019.06.110>.

References

- [1] R.J. Lagow, et al., Synthesis of linear acetylenic carbon: the “sp” carbon allotrope, *Science* 267 (1995) 362–367.
- [2] C.S. Casari, A. Milani, Carbyne: from the elusive allotrope to stable carbon atom wires, *MRS Commun.* 8 (2018) 207–219.
- [3] B. Pan, J. Xiao, J. Li, P. Liu, C. Wang, G. Yang, Carbyne with finite length: the one-dimensional sp carbon, *Sci. Adv.* 1 (2015) e1500857.
- [4] S. Heeg, L. Shi, L.V. Poulikakos, T. Pichler, L. Novotny, Carbon Nanotube chirality determines properties of encapsulated linear carbon chain, *Nano Lett.* 18 (2018) 5426–5431.
- [5] M. Liu, V.I. Artyukhov, H. Lee, F. Xu, B.I. Yakobson, Carbyne from first principles: chain of C atoms, a nanorod or a nanorope? *ACS Nano* 7 (2013) 10075–10082.
- [6] M. Wang, S. Lin, Ballistic: thermal transport in carbyne and cumulene with micron-scale spectral acoustic phonon mean free path, *Sci. Rep.* 5 (2015) 18122.
- [7] Y. Zhu, H. Bai, Y. Huang, Electronic property modulation of one dimensional extended graphdiyne nanowires from a first-principle crystal orbital view, *Chem. Open* 5 (2016) 78.
- [8] S. Tongay, R.T. Senger, S. Dag, S. Ciraci, *Ab-initio* electron transport calculations of carbon based string structures, *Phys. Rev. Lett.* 93 (2004) 136404.
- [9] Z. Zanolli, G. Onida, J.C. Charlier, Quantum spin transport in carbon chains, *ACS Nano* 4 (2010) 5174.
- [10] N.F. Andrade, et al., Linear carbon chains encapsulated in multiwall carbon nanotubes: resonance Raman spectroscopy and transmission electron microscopy studies, *Carbon* 90 (2015) 172–180.
- [11] W.Q. Neves, et al., Effect of pressure on the structural and electronic properties of linear carbon chains encapsulated in double wall carbon nanotubes, *Carbon* 133 (2018) 446–456.
- [12] X. Zhao, Y. Ando, Y. Liu, M. Jinno, T. Suzuki, Carbon nanowire made of a long linear carbon chain inserted inside a multiwalled carbon nanotube, *Phys. Rev. Lett.* 90 (2003) 187401.
- [13] D.W. Boukhvalov, I.S. Zhidkov, E.Z. Kurnaev, E. Fazio, S.O. Cholakh, L. D’Urso, Atomic and electronic structures of stable linear carbon chains on Ag-nanoparticles, *Carbon* 128 (2018) 296–301.
- [14] E. Kano, M. Takeguchi, J. Fujita, A. Hashimoto, Direct observation of Pt-terminating carbyne on graphene, *Carbon* 80 (2014) 382–386.
- [15] Q. Sun, et al., Bottom-up synthesis of metalated carbyne, *J. Am. Chem. Soc.* 138 (2016) 1106–1109.
- [16] M. Kijima, Y. Sakai, H. Shirakawa, Electrochemical synthesis of carbyne catalyzed by nickel complex, *Synth. Met.* 71 (1995) 1837–1840.
- [17] W. Chalifoux, R.R. Tykwinski, Synthesis of polyynes to model the sp-carbon allotrope carbyne, *Nat. Chem.* 2 (2010) 967–971.
- [18] C. Jin, H. Lan, L. Peng, K. Suenaga, S. Iijima, Deriving carbon atomic chains from graphene, *Phys. Rev. Lett.* 102 (2009) 205501.
- [19] V. Scuderi, S. Scalese, S. Bagiante, G. Compagnini, L. D’Urso, V. Privitera, Direct observation of the formation of linear C chain/carbon nanotube hybrid systems, *Carbon* 47 (2009) 2112–2142.
- [20] C. Zhao, R. Kitaura, H. Hara, S. Irle, H. Shinohara, Growth of linear carbon chains inside thin double-wall carbon nanotubes, *Phys. Chem. C* 115 (2011) 13166–13170.
- [21] J. Zhang, et al., Synthesis and transformation of linear adamantane assemblies inside carbon nanotubes, *ACS Nano* 6 (2012) 8674–8683.
- [22] L. Shi, et al., Confined linear carbon chains as a route to bulk carbyne, *Nat. Mater.* 15 (2016) 634–639.
- [23] L. Sheng, A. Jin, L. Yu, K. An, Y. Ando, X. Zhao, A simple and universal method for fabricating linear carbon chains in multiwalled carbon nanotubes, *Mater. Lett.* 81 (2012) 222–224.
- [24] J.R. Rostrup-Nielsen, Production of synthesis gas, *Catal. Today* 18 (1993) 305–324.
- [25] H. Schulz, Short history and present trends of Fischer-Tropsch synthesis, *Appl. Catal. Gen.* 186 (1999) 3–12.
- [26] V. Jourdain, C. Bichara, Current understanding of the growth of carbon nanotubes in catalytic chemical vapour deposition, *Carbon* 58 (2013) 2–39.
- [27] A.C.T. van Duin, S. Dasgupta, F. Lorant, W.A. Goddard III, ReaxFF: a reactive force field for hydrocarbons, *J. Phys. Chem. A* 105 (2001) 9396–9409.
- [28] C. Zou, Y.K. Shin, A.C.T. van Duin, H. Fang, Z.-K. Liu, Molecular dynamics simulations of the effects of vacancies on nickel self-diffusion, oxygen diffusion and oxidation initiation in nickel, using the ReaxFF reactive force field, *Acta Mater.* 83 (2015) 102–112.
- [29] G. Chen, et al., Chemically doped double-walled carbon nanotubes: cylindrical molecular capacitors, *Phys. Rev. Lett.* 90 (2003) 257403.
- [30] H. Shiozawa, et al., Nickel clusters embedded in carbon nanotubes as high performance magnets, *Sci. Rep.* 5 (2015) 15033.
- [31] H.J.C. Berendsen, J.P.M. Postma, W.F. van Gunsteren, A. Di Nola, J.R. Haak, Molecular dynamics with coupling to an external bath, *J. Chem. Phys.* 81 (1984) 3684–3690.
- [32] G. Bussi, D. Donadio, M. Parrinello, Canonical sampling through velocity-rescaling, *J. Chem. Phys.* 126 (2007) 014101.
- [33] Y. Deng, S.W. Cranford, Mapping temperature and confinement dependence of carbyne formation within carbon nanotubes, *Carbon* 141 (2019) 209–217.
- [34] G. Kresse, J. Furthmüller, Efficiency of ab-initio total energy calculations for metals and semiconductors using a plane-wave basis set, *Comput. Mater. Sci.* 6 (1996) 15.
- [35] G. Kresse, J. Furthmüller, Efficient iterative schemes for ab initio total-energy calculations using a plane-wave basis set, *Phys. Rev. B* 54 (1996) 11169.
- [36] B. Hammer, L. Hansen, J. Norskov, Improved adsorption energetics within density-functional theory using revised Perdew-Burke-Ernzerhof functionals, *Phys. Rev. B* 59 (1999) 7413–7421.
- [37] E. Blochl, Projector augmented-wave method, *Phys. Rev. B* 50 (1994) 17953.
- [38] G. Kresse, D. Joubert, From ultrasoft pseudopotentials to the projector augmented-wave method, *Phys. Rev. B* 59 (1999) 1758.
- [39] K.-M. Ho, et al., *Phys. Rev. Lett.* 49 (1982) 673–676.
- [40] C.-L. Fu, et al., *Phys. Rev. B* 28 (1983) 5480–5486.
- [41] J.P. Perdew, K. Burke, M. Ernzerhof, Generalized gradient approximation made simple, *Phys. Rev. Lett.* 77 (1996) 3865.
- [42] J.P. Perdew, K. Burke, M. Ernzerhof, Erratum: generalized gradient approximation made simple, *Phys. Rev. Lett.* 78 (1997) 1396.
- [43] A. Tkatchenko, M. Scheffler, Accurate molecular van Der Waals interactions from ground-state electron density and free-atom reference data, *Phys. Rev. Lett.* 102 (2009) 073005.
- [44] G. Henkelman, B.P. Uberuaga, H.A. Jonsson, Climbing image nudged elastic band method for finding saddle points and minimum energy paths, *J. Chem. Phys.* 113 (2000) 9901–9904.
- [45] S. Lehwald, H. Ibach, Decomposition of hydrocarbons on flat and stepped Ni(111) surfaces, *Surf. Sci.* 89 (1979) 425–445.
- [46] A. Timoshevskii, S. Kotrechko, Y. Matviychuk, Atomic structure and mechanical properties of carbyne, *Phys. Rev. B* 91 (2015) 245434.
- [47] S.E. Muller, A.K. Nair, Carbyne as a fiber in metal-matrix nanocomposites: a first principle study, *Comput. Mater. Sci.* 159 (2019) 187–193.
- [48] J. Januszewski, R.R. Tykwinski, Synthesis and properties of long $[n]$ cumulenes ($n \geq 5$), *Chem. Soc. Rev.* 43 (2014) 3184.
- [49] V.I. Artyukhov, M. Liu, B.I. Yakobson, Mechanically induced metal-insulator transition in carbyne, *Nano Lett.* 14 (2014) 4224–4229.
- [50] C. Ming, F.-X. Meng, X. Chen, J. Zhuang, X.-J. Ning, Tuning the electrical and optical properties of monatomic carbon chains, *Carbon* 68 (2014) 487–492.
- [51] L. Shi, et al., Electronic band gaps of confined linear carbon chains ranging from polyene to carbyne, *Phys. Rev. Mater.* 1 (2017), 075601.